Bioorganic & Medicinal Chemistry 18 (2010) 3270–3278

Contents lists available at ScienceDirect

Bioorganic & Medicinal Chemistry

journal homepage: www.elsevier.com/locate/bmc

3,5-Diaryl-1*H*-pyrazole as a molecular scaffold for the synthesis of apoptosis-inducing agents

Arthur Y. Shaw [a,e,*], Hao-Han Liau [a], Pei-Jung Lu [b], Chia-Ning Yang [c], Chien-Hsing Lee [b], Jun-Yan Chen [d], Zhigang Xu [e], Gary Flynn [e]

[a] Department of Chemistry, Tamkang University, Taipei 251, Taiwan
[b] Institute of Clinical Medicine, National Cheng Kung University, Tainan 701, Taiwan
[c] Institute of Biotechnology, National University of Kaohsiung, Kaohsiung 700, Taiwan
[d] Department of Life Science, National University of Kaohsiung, Kaohsiung 700, Taiwan
[e] Department of pharmacology and Toxicology, College of Pharmacy, The University of Arizona, Tucson, AZ 85724, USA

ARTICLE INFO

Article history:
Received 13 January 2010
Revised 8 March 2010
Accepted 9 March 2010
Available online 16 March 2010

Keywords:
3,5-Diaryl-1*H*-pyrazole
Molecular scaffold
Apoptosis-inducing agent
Mitochondrial apoptotic pathway
Structure–activity relationship

ABSTRACT

The scaffold of 3,5-diaryl-1*H*-pyrazole was selected as a molecular template to synthesize novel growth-inhibitory agents in the present study. Our findings suggested that analogs bearing electron-withdrawing groups on one ring while electron-donating groups on another reveal significant activities. In particular, **26** bearing a 1,1′-biphenyl moiety displayed the most potent activity against OVCA, SW620, H460 and AGS cells with GI_{50} values of 0.67, 0.89, 0.73 and 0.79 μM, respectively. The mechanistic study revealed that 26-mediated apoptosis-inducing effect on OVCA cells was, in part, attributed to the inhibition of protein kinase B/Akt activity, accompanied by the mitochondrial apoptotic pathway through the activation of caspase-9, caspase-3, as well as the cleavage of protein poly(ADP-ribose) polymerase (PARP) and DNA fragmentation. Further structure–activity relationship study employed by Comparative Molecular Field Analysis (CoMFA) was carried out with q^2 and R^2 values of 0.671 and 0.846, respectively.

1. Introduction

Apoptosis, or programmed cell death, is the prevalent mechanism for cellular development and differentiation. Deregulation of apoptosis is widely believed to be involved in a variety of human diseases, including cancer, autoimmune diseases, and neurodegeneration disorders.[1,2] Appreciable progress in elucidating molecular components of the apoptotic machinery have resulted in the identification of many molecular targets for the development of new drugs with pro- and anti-apoptotic activity to treat different diseases including cancer. So far, two principle apoptotic pathways are identified, the death receptor (or extrinsic) and the mitochondria (or intrinsic) pathways, both of which involve the activation of a family of cysteine proteases with aspartate specificity, called caspases, as the executioners of apoptosis.[3,4] Based on the urgent need for cancer patients, developing small molecules that activate and induce apoptosis is a promising strategy for the treatment of cancer.

The pyrazole scaffold has drawn a great deal of attention due to its contributions in biological and pharmacological fields regardless of scarcity in nature.[5] For example, N-substituted pyrazoles such as pirazolac is known as non-steroidal anti-inflammatory drugs (NSAIDs).[6] Celecoxib, a selective cyclooxygenase-2 (COX-2) inhibitor, is clinically used for the therapy of osteoarthritis, rheumatoid arthritis, acute pain and so on (Fig. 1).[7] On the other hand, N-substituted pyrazoles have also been developed as inhibitors of p38 mitogen-activated protein kinase, SERMs (selective estrogen receptor modulators) for the treatment of cancer cells.[8,9] Recently, several 3,5-diary-1*H*-pyrazoles were reported as inhibitors of monoamine oxidases.[10] In light of our research on the development of small molecules targeting cancer cells, the present study we take advantage of 3,5-diaryl-1*H*-pyrazole (Fig. 1) as a molecular scaffold to synthesize a series of derivatives for the evaluation of their growth-inhibitory effect against carcinoma cell lines.

2. Results and discussion

2.1. Synthesis of 3,5-diaryl-1*H*-pyrazoles 1–33

The preparation of 3,5-diaryl-1*H*-pyrazole was originally from the cyclization of 1,3-diketone and hydrazine in 1893.[11] Although several methods have been developed, some tedious procedures or more reagents are required to handle with. In the present study, we initially carried out the nucleophilic substitution by the treatment of commercially available acetophenone and benzoyl chloride in the presence of strong base *n*-BuLi that afforded

* Corresponding author at: 1703 E. Mabel St., Tucson, AZ 85721, USA.
E-mail address: shaw.299@gmail.com (A.Y. Shaw).

0968-0896/$ - see front matter © 2010 Elsevier Ltd. All rights reserved.
doi:10.1016/j.bmc.2010.03.016

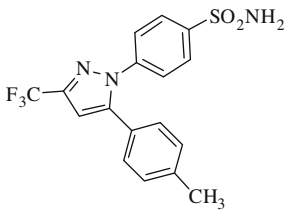

Celecoxib

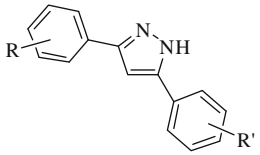

3,5-diaryl-*1H*-pyrazole

Figure 1. Chemical structures of pyrazole derivatives.

1,3-diketone. Without further purification, 1,3-diketone was subjected to undergo cyclization with hydrazine in refluxed ethanol to give 3,5-diaryl-1*H*-pyrazole.[12] The acetophenone was deprotonated by *n*-BuLi to generate a nucleophilic enolate, followed by the nucleophilic substitution with benzoyl chloride to give 1,3-diketone. Nevertheless, some side products have been found during the preparation of 1,3-diketone. We assumed that side products might be attributed to the self-condensation of acetophenone. Moreover, *n*-BuLi was also found to serve as a nucleophile to attack benzoyl chloride that afforded 1-aryl-pentan-1-ones. As a result, we took advantage of a more updated synthetic method with slight modifications according to the report in the literature.[13] As shown in Scheme 1, both 2 equiv of acetophenone and lithium bis(trimethylsilyl)amide (LiHMDS) and 1 equiv of benzoyl chloride were charged in the toluene. Without further purification, the reaction solution was evaporated in vacuo to obtain 1,3-diketone, followed by the addition of hydrazine in refluxed ethanol to synthesize 3,5-diaryl-1*H*-pyrazoles. The strong base LiHMDS used in this method is more advantageous than *n*-BuLi thanks to its poor nucleophilicity. Consequently, we synthesized a series of 3,5-diaryl-1*H*-pyrazoles, some of which were subjected to proceed hydrogenation or demethylation reaction to afford the corresponding products (Scheme 2).

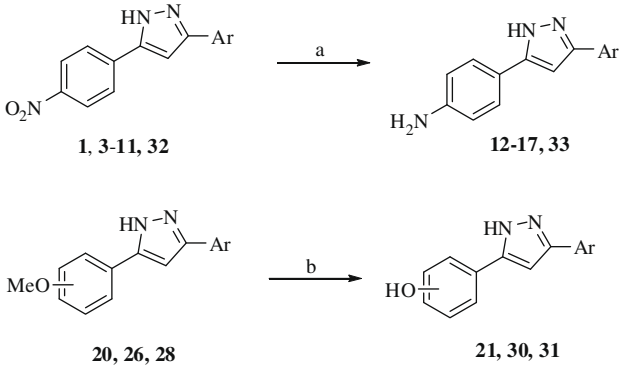

Scheme 2. Reagents and conditions: (a) Pd/C, H_2, MeOH, rt, 16 h; (b) BBr_3, DCM.

2.2. Growth inhibition of 1–33 against four carcinoma cells

The evaluation of growth-inhibitory activity of 3,5-diaryl-1*H*-pyrazoles **1**–**33** was examined on a panel of human carcinoma cell lines, including OVCA (ovarian carcinoma cell), SW620 (colorectal adenocarcinoma cell), H460 (large lung carcinoma cell) and AGS (gastric carcinoma cell). The MTT assay was employed for growth inhibition studies and the GI_{50} values are summarized in Tables 1–3. The tested compound concentration causing a 50% cell growth inhibition (GI_{50}) was determined by interpolation from dose–response curves[14].

As shown in Table 1, analogs **1–11** contain an electron-withdrawing nitro group at 4- or 3-position on one benzene ring while various substituents on another. Among four carcinoma cell lines, OVCA and H460 cell lines seemed to be more sensitive in response to the growth inhibition with GI_{50} values between 5.8 and 28.9 μM. Compared to the mono-substituted counterparts, disubstituted **6** (3,4-dimethoxy) and **7** (3,4-methoxydioxy) displayed higher activities against most cell lines. Interestingly, substituents at 4-position such as **6–10** showed better activity than the counterparts **1–5** against SW620 cell line.

Upon the reduction of the nitro group in **1** and **3–7**, the corresponding counterparts **12–17** were generated, most of which did not show any growth-inhibitory effects. Nevertheless, **17** (4-NH_2) showed an improved growth-inhibitory effect against OVCA and H460 cell lines in comparison with the counterpart **11** (4-NO_2) with GI_{50} values of 18.6 and 21.5 μM, respectively (Table 2). These results indicated that either electron-donating or electron-withdrawing group simultaneously present on both sides would result in a precipitous loss in potency. On the other hand, as the amino group in **17** (4-NH_2) was replaced with a dimethylamino group in **18** (4-NMe_2), a dramatic decrease in activity was observed. This finding suggests that the amino group bearing hydrogen bond-donating character plays an important role for activity.

It is worthwhile to notice that **19** without any substituents on one side exhibited more activity than **22–24** with substituents on both sides. In addition to the electronic modulations, the steric factor demanded modification was further investigated based on **19**. As shown in Table 3, a series of 1,1′-biphenyl analogs **26–33** introduced a phenyl at 2-position on one side revealed a tremendous enhancement in potency. Remarkably, **26** displayed the most potent activity against OVCA, SW620, H460 and AGS cell lines with GI_{50} values of 0.67, 0.89, 0.73 and 0.79 μM, respectively. On the contrary, upon the replacement of the methoxy group in **26** with a hydroxyl group in **31**, a 10-fold decrease in activity was clearly observed. Similarly, as the nitro group in **32** was transformed into an amino group to generate the counterpart **33**, a significant loss in potency was demonstrated as well. Together, these results indicate that a hydrogen-bond donor such as hydroxyl and amino groups at 4-position of benzene ring potentially counteract their growth-inhibitory effect. On the other hand, as 4-methoxygroup was replaced with 2- or 3-methoxy group, a precipitous decreases in

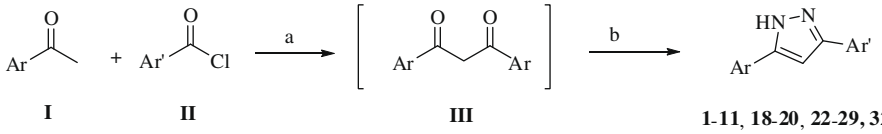

Scheme 1. Reagents and conditions: (a) LiHMDS, toluene, 0 °C, 2 h; (b) NH_2NH_2·HCl, EtOH, reflux, 16 h.

Table 1
Chemical structures and GI_{50} values of 3,5-diarylpyrazoles **1–11**

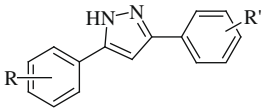

R = 4-NO_2 **1**, **3**-**11**
R = 3-NO_2 **2**

Entry	R′	GI_{50}[a] (μM)			
		OVCA	SW620	H460	AGS
1	Hydrogen	7.2 ± 1.8	ND[b]	10.2 ± 1.9	ND
2	Hydrogen	5.8 ± 0.4	ND	6.1 ± 2.6	11.4 ± 0.9
3	2-Methoxy	11.7 ± 0.9	ND	20.5 ± 4.7	ND
4	3-Methoxy	19.1 ± 5.1	ND	11.2 ± 2.4	ND
5	4-Methoxy	27.3 ± 4.3	14.3 ± 1.8	18.3 ± 5.6	ND
6	3,4-Dimethoxy	28.9 ± 5.3	26.4 ± 1.1	17.9 ± 4.8	ND
7	3,4-Methylenedioxy	10.8 ± 1.8	23.5 ± 3.4	8.9 ±2.2	13.1 ± 1.3
8	4-Fluoro	ND	18.1 ± 1.2	ND	18.3 ± 0.3
9	4-Chloro	ND	12.2 ± 1.8	20.7 ± 6.2	24.1 ± 0.8
10	4-Bromo	17.5 ± 3.2	28.6 ± 2.9	ND	14.6 ± 0.5
11	4-Trifluoromethyl	ND	ND	ND	ND

[a] GI_{50} values are presented as the mean ± SEM (standard error of the mean) from four to six separated experiments.
[b] ND indicated that no appreciable growth inhibition was observed upon treatment of maximal concentration at 40 μM.

potency was also observed, suggesting that substituents at 4-position exhibit a favorable interaction for growth inhibitor. In addition, 2-hydroxy substituted **30** showed at least twofold more potent than the counterpart **28** with 2-methoxy group. We speculate the improved activity might due to the intramolecular hydrogen bonding between the hydroxyl group and nitrogen atom on the pyrazole core that maintains the rigidity of structure for activity.

Table 3
Chemical structures and GI_{50} values of 3,5-diaryl-1*H*-pyrazoles **26–33**

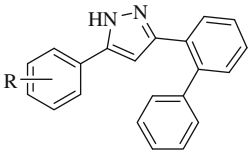

26-33

Entry	R	GI_{50}[a] (μM)			
		OVCA	SW620	H460	AGS
26	4-OMe	0.67 ± 0.1	0.89 ± 0.12	0.73 ± 0.11	0.79 ± 0.08
27	4-CF_3	2.75 ± 0.1	ND[b]	ND	6.9 ± 0.7
28	2-OMe	14.2 ± 1.1	ND	9.1 ± 2.5	ND
29	3-OMe	5.8 ± 1.3	ND	8.7 ± 1.4	7.5 ± 0.8
30	2-OH	5.8 ± 0.4	10.6 ± 0.7	4.6 ± 1.2	7.5 ± 0.5
31	4-OH	6.2 ± 0.6	25.9 ± 4.6	6.9 ± 1.5	9.2 ± 0.6
32	4-NO_2	3.4 ± 0.4	12.2 ± 1.2	2.7 ± 1.1	1.2 ± 0.1
33	4-NH_2	17.9 ± 1.1	ND	8.2 ± 1.3	8.4 ± 0.6

[a] GI_{50} values are presented as the mean ± SEM (standard error of the mean) from four to six separated experiments.
[b] ND indicated that no appreciable growth inhibition was observed upon treatment of maximal concentration at 40 μM.

2.3. Induction of apoptosis by 26 and 27 through caspase-dependent pathways and inactivation of protein kinase B/Akt

To demonstrate whether the cell growth inhibition was related to cell cycle regulation and apoptosis, **26** and **27** were selected for further mechanistic study on OVCA cells. As indicated in the flow cytometric analysis (Fig. 2), accumulation of sub-G1 arrest in response to **26**- and **27**-treated cells was clearly observed in a dose-dependent manner. Upon the exposure of OVCA cells to **26** at 1.2, 2.5 and 5.0 μM, the substantial sub-G1 arrest was detected with 14.97%, 20.53% and 32.05%, respectively. Similarly, OVCA treated with **27** at 1.2, 2.5 and 5.0 μM also led to the increased

Table 2
Chemical structures and GI_{50} values of 3,5-diarylpyrazoles **12–25**

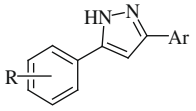

R = 4-NH_2 **12-17** R = 4-NMe_2 **18**
R = 4-OMe **19, 20**, **22-25** R = 4-OH **21**

Entry	Ar	GI_{50}[a] (μM)			
		OVCA	SW620	H460	AGS
12	Phenyl	ND[b]	25.4 ± 2.4	26.7 ± 0.9	ND
13	2-Methoxyphenyl	ND	21.1 ± 1.2	ND	ND
14	3-Methoxyphenyl	ND	ND	ND	ND
15	4-Methoxyphenyl	ND	ND	ND	ND
16	3,4-Dimethoxyphenyl	ND	ND	ND	ND
17	4-Trifluoromethylphenyl	18.6 ± 5.5	ND	21.5 ± 3.1	ND
18	4-Trifluoromethylphenyl	ND	ND	ND	ND
19	Phenyl	9.9 ± 1.9	27.2 ± 3.8	10.4 ± 3.4	11.3 ± 0.7
20	4-trifluoromethylphenyl	22.8 ± 3.5	11.2 ± 1.1	ND	14.8 ± 0.3
21	4-Trifluoromethylphenyl	9.2 ± 1.0	19.6 ± 1.8	20.1 ± 2.4	9.8 ± 0.9
22	4-Fluorophenyl	14.0 ± 2.7	ND	ND	ND
23	4-Chlorophenyl	12.8 ± 2.9	ND	11.6 ± 4.1	ND
24	4-Bromophenyl	20.7 ± 2.1	ND	27.1 ± 3.9	ND
25	2-Naphthyl	17.5 ± 1.6	26.9 ± 2.3	13.2 ± 1.0	19.0 ± 0.4

[a] GI_{50} values are presented as the mean ± SEM (standard error of the mean) from four to six separated experiments.
[b] ND indicated that no appreciable growth inhibition was observed upon treatment of maximal concentration at 40 μM.

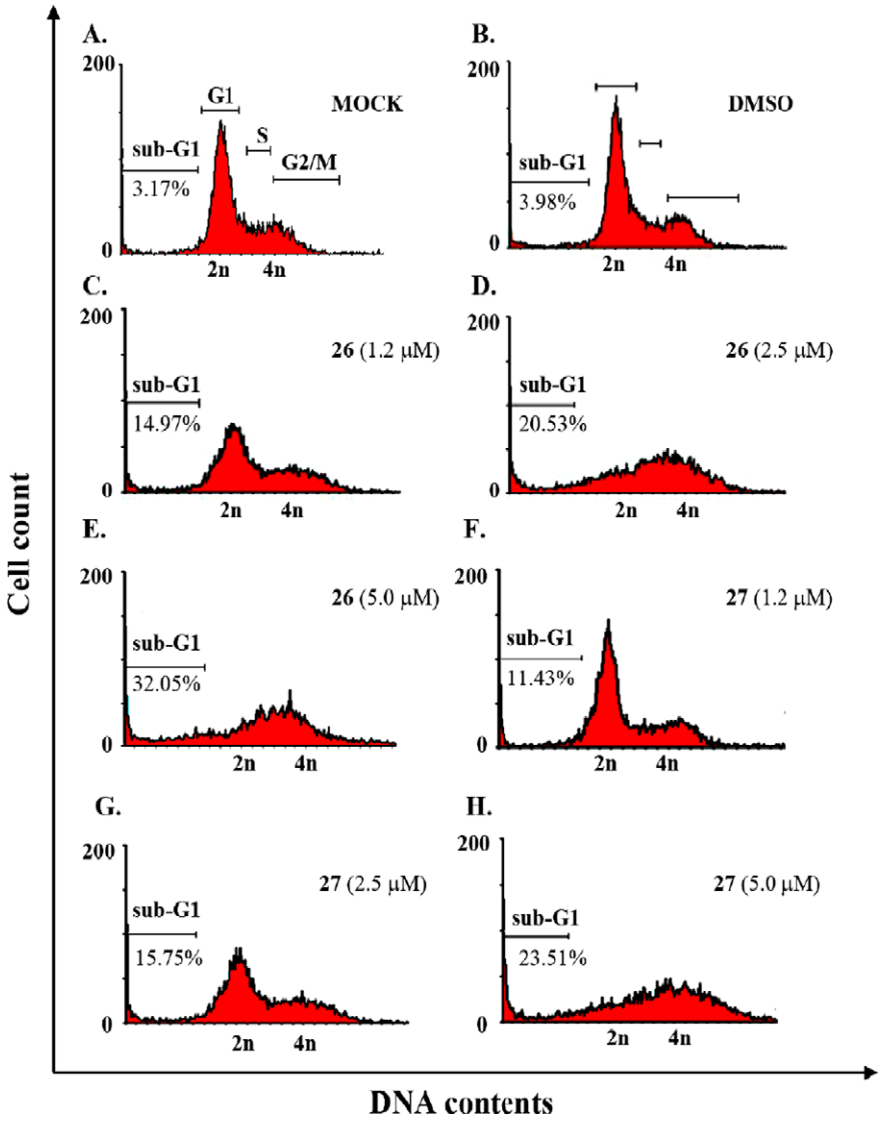

Figure 2. Flow cytometric analysis of OVCA cells. Cells were harvested after 24 h treatment and followed by fixation, propidium iodide staining prior to the flow cytometric analysis. Sub-G1 phase indicated the DNA fragmentation and cell death. Exposure of OVCA cells to **26** at 1.2, 2.5 and 5.0 μM caused the sub-G1 phase arrest with 14.97%, 20.53% and 32.05%, respectively. Similarly, OVCA cells exposed to **26** at 1.2, 2.5 and 5.0 μM caused the sub-G1 phase arrest with 11.43%, 15.75% and 23.51%, respectively. (A) Untreated OVCA cells were taken as blank group; (B) cells were treated with 0.5% DMSO as the control; (C) treatment of **26** at 1.2 μM; (D) treatment of **26** at 2.5 μM; (E) treatment of **26** at 5.0 μM; (F) treatment of **27** at 1.2 μM; (G) treatment of **27** at 2.5 μM; (H) treatment of **27** at 5.0 μM.

sub-G1 arrest with 11.43%, 15.75% and 23.51%, respectively. These findings suggested that growth inhibition of OVCA cells mediated by **26** and **27** may cause DNA fragmentation and cell death.

On the other hand, Western blot of cytosolic extracts prepared from **26**- and **27**-treated OVCA cells for 16 h revealed cleavage of the 116-kDa protein poly(ADP-ribose) polymerase (PARP) to generate 89-kDa fragment (Fig. 3). The results were consistent with the activation of pro-apoptotic caspase-3, as shown by the increased level of 17/19-kDa cleaved caspase-3. Moreover, the activation of the upstream caspase-9 was also monitored by the elevated levels of 35/37-kDa cleaved caspase-9. Taken together, we concluded that the apoptosis-inducing effect on OVCA cells mediated by **26** and **27** was through the mitochondrial apoptotic pathway.

Aberrant function of PI3K/Akt signaling pathway contributes to cell proliferation and survival in a variety of neoplasms including ovarian cancer. Akt is overexpressed in a substantial number of ovarian cancers, resulting in the constitutive activation of signaling pathway indicated by phosphorylation of Akt in vitro and in vivo.[15] In addition to the elucidation of mitochondrial apoptotic pathway, we attempted to examine the effect on the phosphorylation state of Akt due to its significance in OVCA cell survival. As indicated in Figure 3, the reduction of phospho-Akt level was clearly observed, indication deactivation of Akt was in response to **26** and **27** treatment. Additionally, the more potent inhibitory effect on Akt activity of **26** over **27** coincided with growth-inhibitory activity with GI_{50} values of 0.67 and 2.75 μM, respectively. These results suggested the induction of apoptosis by **26** and **27** in OVCA ovarian cancer cells was, in part, attributable to the inhibition of Akt activity.

2.4. Structure–activity relationship study on OVCA cells

Structure–activity relationship analysis was further examined on OVCA cells. Comparative Molecular Field Analysis (CoMFA) was employed by software Sybyl 8.1 to characterize structure–activity relationships in this study. Our final training set model and coefficients such as non-validation R^2 and *F*-value were ob-

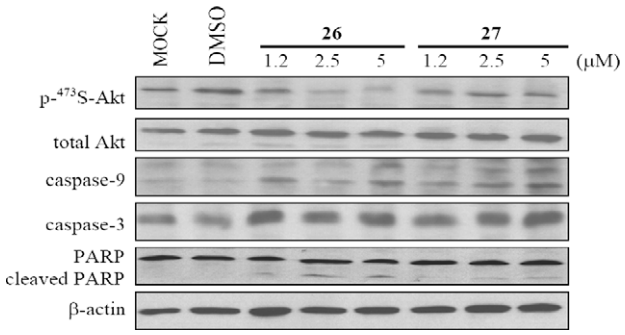

Figure 3. Induction of apoptosis in OVCA cells by **26** and **27**. Induction of poly(ADP-ribose) polymerase (PARP) cleavage by **26** and **27** at the indicated concentrations after 16 h of treatment. PARP proteolysis to the apoptosis-specific 85-kDa fragment was monitored by western blotting. The appearance of a 89-kDa fragment coincided with the activation of caspase-3, as shown by the increased level of the 17/19-kDa cleaved caspase-3. The activation of the upstream caspase-9 was also observed with the increased level of the 35/37-kDa cleaved caspase-9, indicating the mitochondrial apoptotic pathway was involved. The phosphorylation status of Akt was also determined by immunoblot analysis with phosphospecific antibody. Unphosphorylated Akt, as immunostained by anti-Akt antibody, was used as internal standard for the comparison of phospho-Akt level among samples of different preparations.

tained by using the optimal number of components and all the data points in the training set. The cross-validated q^2 value with 0.671 and the subsequent non-validation R^2 value with 0.846 meet the criteria ($q^2 \geqq 0.5$; $R^2 \geqq 0.8$) that indicate the constructed model is internally predictive and accountable. The contributions for steric and electrostatic fields are 0.459 and 0.561, respectively. As shown in Figure 4A, all analogs were aligned to the pyrazole core as specified in stick. The steric field (in yellow/green for unfavorable/favorable contours, Fig. 4B) and electrostatic field (in blue/red for positive/negative charge favorable contours, Fig. 4C) projected onto **32**. In steric field model, three steric unfavorable contours near C-2′, C-3′, and C-4′ greatly restrict the modifications around the ring A moiety. Accordingly, **1** shows a higher activity (GI_{50}, 7.2 μM) compared to **3** (GI_{50}, 11.7 μM) bearing a methoxy group on C-2′ and **6** (GI_{50}, 28.9 μM) with methoxy groups on C-3′ and C-4′. The steric favorable contour centering on C-6′ is amenable for modifications evidenced by comparing **25** (GI_{50}, 17.5 μM) and **26** (GI_{50}, 0.67 μM) with a bulky phenyl group on C-6′. A steric unfavorable contour is located at C-4″ position on the ring B moiety, which explains the different location of a nitro group, such as C-4″ in **1** and C-3″ in **2**, responsible for different activities with GI_{50} values of 7.2 and 5.8 μM, respectively. In electrostatic field model (Fig. 4C), the blue contour around C-2′ suggests a positively charged substituent to increase activity. As a consequence, **3** (GI_{50}, 11.7 μM) with a partial negatively charged methoxy oxygen atom nearby the blue contour has a lower activity compared to **1** without substituent. The mixed one blue contour and two red contours around C-4″ correspondingly match a nitro group composed of a positively charged nitrogen atom and two negatively charged oxygen atoms. It interprets the dramatic discrepancy in activity between **1** (4-NO_2, GI_{50}, 7.2 μM) and **12** (4-NH_2, GI_{50}, ND) with distinct charge distribution on C-4″.

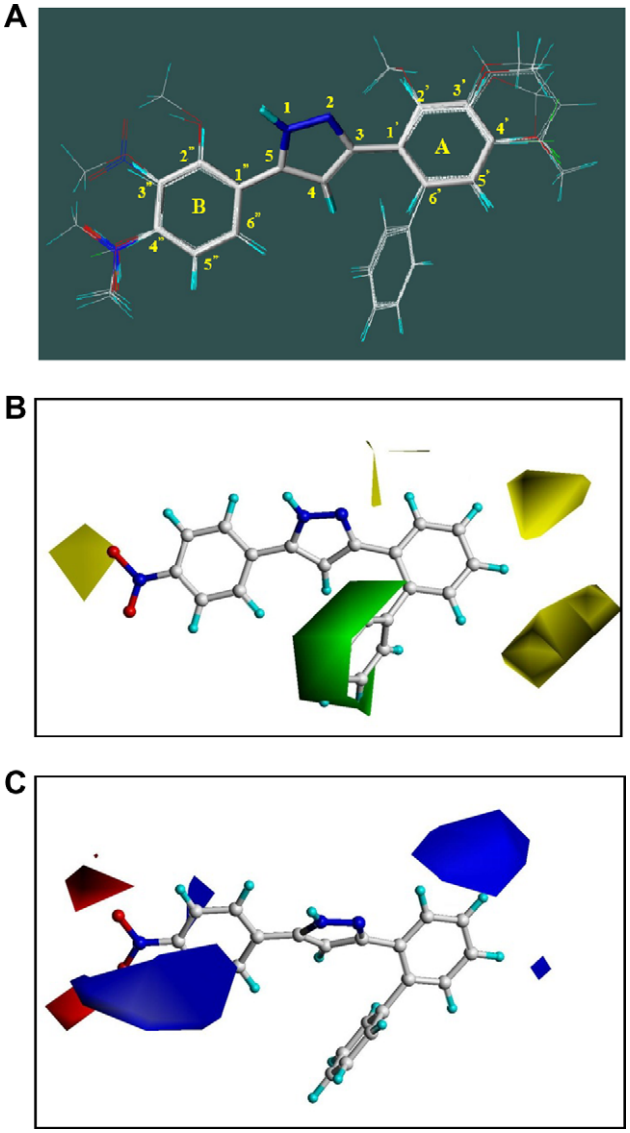

Figure 4. 3D-QSAR study on OVCA cells. Comparative Molecular Field Analysis (CoMFA) was employed by software Sybyl 8.1 to characterize structure–activity relationships. (A) Alignment of 3,5-diaryl-1*H*-pyrazoles **1–33** to the pyrazole core specified in stick. (B) Steric field projected on **32**: yellow contour indicate bulky groups decrease activity (contribution level of 80%), whereas green contours indicate bulky groups increase activity (contribution level of 20%); (C) Electrostatic field projected on **32**: red contours indicate negatively charged groups increase activity (contribution level of 20%), whereas blue contours indicate positively charged groups increase activity (contribution level of 80%).

3. Conclusions

In the present study, a more updated two-step synthesis of 3,5-diaryl-1*H*-pyrazoles was carried out. With 33 analogs in hand, growth inhibition evaluation on a panel of four carcinoma cells was examined. Our findings suggest that analogs bearing an electron-withdrawing group on one side while an electron-donating group on another exhibited better growth-inhibitory effect. In addition, we found that dramatic enhancement in potency was observed upon the introduction of a phenyl moiety at 2-position on one side. Particularly, **26** bearing a 1,1′-biphenyl moiety exhibited the most potent activity against OVCA, SW620, H460 and AGS cells with GI_{50} values of 0.67, 0.89, 0.73 and 0.79 μM, respectively. Furthermore, the mechanistic study on OVCA cells demonstrated that growth inhibition mediated by **26** and **27** was, in part, attributed to the inhibition of intracellular Akt activity. The mitochondrial apoptotic pathway was also evidenced by the activation of caspase-9, caspase-3, cleavage of protein poly(ADP-ribose) polymerase (PARP) and DNA fragmentation. The structure–activity relationship analysis employed by Comparative Molecular Field Analysis (CoMFA) model was generated with q^2 and R^2 values of 0.671 and 0.846, respectively, suggesting its predictivity and accountability warranted for further study.

4. Experimental

4.1. Synthesis

Chemical reagents and organic solvents were purchased from TCI and Alfa Aesar unless otherwise mentioned. Melting points were determined by Fargo MP-2D. Nuclear magnetic resonance spectra (^{1}H and ^{13}C NMR) were measured on a Bruker AC-300 instrument. Chemical shifts (δ) are reported in ppm relative to the TMS peak. Mass spectra were obtained by FAB on a Jeol JMS-700 instrument. Flash column chromatography was performed with silica gel (230–400 mesh).

4.1.1. 5-(4-Nitrophenyl)-3-phenyl-1*H*-pyrazole (1)

To an ice-cooled solution of acetophenone (0.48 g, 4.0 mmol) in toluene (20 ml) was added a solution of LiHMDS (4.2 ml, 1.0 M in THF, 4.2 mmol), the resulting mixture was stirred for 20 min, followed by the addition of 4-nitrobenzoyl chloride (0.37 g, 2.0 mmol) then allowed to stir at room temperature for 2 h. The reaction mixture was diluted with ethyl acetate (40 ml), washed with water (50 ml), brine (50 ml), and dried over $MgSO4_{(s)}$ and evaporated in vacuo to obtain the crude 1,3-diketone intermediate. Without further purification, the 1,3-diketone and hydrazine hydrochloric acid (NH_2NH_2·HCl, 10.0 mmol) were added to ethanol (80 ml) solution and the resulting mixture was stirred at reflux for 16 h. The reaction mixture was evaporated in vacuo to obtain the residue, followed by the addition of ethyl acetate (50 ml), washed with water (50 ml), brine (50 ml). The organic layer was dried over $MgSO_4$, evaporated in vacuo and purified with silica gel chromatography (ethyl acetate/hexane = 1:9) to afford 5-(4-nitrophenyl)-3-phenyl-1*H*-pyrazole (**1**). Mp 281 °C. ^{1}H NMR (300 MHz, DMSO-d_6) δ 7.38 (t, J = 7.3 Hz, 1H), 7.42 (s, 1H), 7.49 (dd, J = 7.6, 7.3 Hz, 2H), 7.84 (d, J = 7.6 Hz, 2H), 8.12 (d, J = 8.6 Hz, 2H), 8.31 (d, J = 8.6 Hz, 2H) ppm. ^{13}C NMR (75 MHz, DMSO-d_6) δ 101.21, 124.19, 125.18, 125.83, 128.22, 128.95, 146.43 ppm. HRMS $(M+1)^+$ calcd for $C_{15}H_{11}N_3O_2$ 266.0885; found 266.0931.

4.1.2. 5-(3-Nitrophenyl)-3-phenyl-1*H*-pyrazole (2)

Compound **2** was synthesized from the procedure described for **1**. Mp 214 °C. ^{1}H NMR (300 MHz, DMSO-d_6) δ 7.36 (t, J = 7.3 Hz, 1H), 7.42 (s, 1H), 7.47 (dd, J = 7.5, 7.3 Hz, 2H), 7.76 (dd, J = 8.0, 7.6 Hz, 1H), 7.84 (d, J = 7.5 Hz, 2H), 8.16 (d, J = 8.0 Hz, 1H), 8.28 (d, J = 7.6 Hz, 1H), 8.66 (s, 1H), 13.61 (br s, NH) ppm. ^{13}C NMR (75 MHz, DMSO-d_6) δ 100.38, 119.20, 122.01, 125.17, 128.35, 129.02, 130.30, 131.32, 135.32, 143.95, 148.35, 149.28 ppm. HRMS $(M)^+$ calcd for $C_{15}H_{11}N_3O_2$ 265.0851; found 265.0848.

4.1.3. 3-(2-Methoxyphenyl)-5-(4-nitrophenyl)-1*H*-pyrazole (3)

Compound **3** was synthesized from the procedure described for **1**. Mp 226 °C. ^{1}H NMR (300 MHz, DMSO-d_6) δ 3.92 (s, 3H), 7.05 (dd, J = 7.5, 7.2 Hz, 1H), 7.15 (d, J = 8.3 Hz, 1H), 7.34 (s, 1H), 7.36 (dd, J = 8.3, 7.2 Hz,1H), 7.77 (d, J = 7.5 Hz, 1H), 8.11 (d, J = 8.8 Hz, 2H), 8.28 (d, J = 8.8 Hz, 2H), 13.27 (br s, NH) ppm. ^{13}C NMR (75 MHz, DMSO-d_6) δ 55.53, 103.27, 111.95, 120.72, 124.17, 125.79, 127.74, 129.70, 139.79, 146.33, 155.78 ppm. HRMS $(M)^+$ calcd for $C_{16}H_{13}N_3O_3$ 295.0957; found 295.0955.

4.1.4. 3-(3-Methoxyphenyl)-5-(4-nitrophenyl)-1*H*-pyrazole (4)

Compound **4** was synthesized from the procedure described for **1**. Mp 233 °C. ^{1}H NMR (300 MHz, DMSO-d_6) δ 3.81 (s, 3H), 6.93 (d, J = 6.7 Hz, 1H), 7.38 (dd, J = 7.2, 6.7 Hz,1H), 7.39 (d, J = 7.2 Hz, 1H), 7.40 (s, 1H), 7.44(s, 1H), 8.11 (d, J = 8.8 Hz, 2H), 8.31 (d, J = 8.8 Hz, 2H), 13.70 (br s, NH) ppm. ^{13}C NMR (75 MHz, DMSO-d_6) δ 55.21, 101.41, 110.60, 113.92, 117.53, 124.19, 125.82, 125.97, 130.11, 146.44, 159.72 ppm. HRMS $(M)^+$ calcd for $C_{16}H_{13}N_3O_3$ 295.0957; found 295.0959.

4.1.5. 3-(4-Methoxyphenyl)-5-(4-nitrophenyl)-1*H*-pyrazole (5)

Compound **5** was synthesized from the procedure described for **1**. Mp 205 °C. ^{1}H NMR (300 MHz, DMSO-d_6) δ 3.79 (s, 3H), 7.04 (d, J = 8.6 Hz, 2H), 7.30 (s, 1H), 7.76 (d, J = 8.6 Hz, 2H), 8.10 (d, J = 8.8 Hz, 2H), 8.30 (d, J = 8.8 Hz, 2H), 13.54 (br s, NH) ppm. ^{13}C NMR (75 MHz, DMSO-d_6) δ 55.22, 100.09, 114.45, 124.10, 125.77, 126.61, 146.35, 159.36 ppm. HRMS $(M)^+$ calcd for $C_{16}H_{13}N_3O_3$ 295.0957; found 295.0963.

4.1.6. 3-(3,4-Dimethoxyphenyl)-5-(4-nitrophenyl)-1*H*-pyrazole (6)

Compound **6** was synthesized from the procedure described for **1**. Mp 194 °C. ^{1}H NMR (300 MHz, DMSO-d_6) δ 3.79 (s, 3H), 3.85 (s, 3H), 7.04 (d, J = 8.2 Hz, 1H), 7.32 (s, 1H), 7.36 (d, J = 8.2 Hz, 1H), 7.43 (s, 1H), 8.10 (d, J = 8.4 Hz, 2H), 8.28 (d, J = 8.4 Hz, 2H), 13.58 (br s, NH) ppm. ^{13}C NMR (75 MHz, DMSO-d_6) δ 55.56, 55.65, 100.29, 109.11, 112.10, 117.75, 121.68, 124.11, 125.75, 140.21, 144.23, 146.34, 149.04, 149.19 ppm. HRMS $(M)^+$ calcd for $C_{17}H_{15}N_3O_4$ 325.1063; found 325.1060.

4.1.7. 3-(Benzo[*d*][1,3]dioxol-5-yl)-5-(4-nitrophenyl)-1*H*-pyrazole (7)

Compound **7** was synthesized from the procedure described for **1**. Mp 249 °C. ^{1}H NMR (300 MHz, DMSO-d_6) δ 6.06 (s, 2H), 7.01 (d, J = 7.6 Hz, 1H), 7.27 (s, 1H), 7.31 (d, J = 7.6 Hz, 1H), 7.37 (s, 1H), 8.07 (d, J = 7.9 Hz, 2H), 8.23 (d, J = 7.9 Hz, 2H), 13.53 (br s, NH) ppm. ^{13}C NMR (75 MHz, DMSO-d_6) δ 100.54, 101.38, 105.66, 108.82, 119.13, 123.04, 124.14, 125.78, 140.11, 143.98, 146.41, 147.40, 147.90, 149.26 ppm. HRMS $(M)^+$ calcd for $C_{16}H_{11}N_3O_4$ 309.0750; found 309.0749.

4.1.8. 3-(4-Fluorophenyl)-5-(4-nitrophenyl)-1*H*-pyrazole (8)

Compound **8** was synthesized from the procedure described for **1**. Mp 302 °C. ^{1}H NMR (300 MHz, DMSO-d_6) δ 7.31 (d, J = 5.2 Hz, 2H), 7.35 (s, 1H), 7.85 (s, J = 5.2 Hz, 2H), 8.09 (d, J = 8.4 Hz, 2H), 8.27 (d, J = 8.4 Hz, 2H), 13.70 (br s, NH) ppm. ^{13}C NMR (75 MHz, DMSO-d_6) δ 101.04, 115.88, 124.11, 125.81, 127.29, 143.12, 163.62 ppm. HRMS $(M)^+$ calcd for $C_{15}H_{10}FN_3O_2$ 283.0757; found 283.0761.

4.1.9. 3-(4-Chlorophenyl)-5-(4-nitrophenyl)-1*H*-pyrazole (9)

Compound **9** was synthesized from the procedure described for **1**. Mp 280 °C. ^{1}H NMR (300 MHz, DMSO-d_6) δ 7.41 (s, 1H), 7.51 (d, J = 8.4 Hz, 2H), 7.85 (d, J = 8.4 Hz, 2H), 8.08 (d, J = 8.7 Hz, 2H), 8.28 (d, J = 8.7 Hz, 2H), 13.74 (br s, NH) ppm. ^{13}C NMR (75 MHz, DMSO-d_6) δ 101.59, 124.22, 125.86, 126.90, 128.96, 132.66, 146.48 ppm. HRMS $(M)^+$ calcd for $C_{15}H_{10}ClN_3O_2$ 299.0462; found 299.0459.

4.1.10. 3-(4-Bromophenyl)-5-(4-nitrophenyl)-1*H*-pyrazole (10)

Compound **10** was synthesized from the procedure described for **1**. Mp 258 °C. ^{1}H NMR (300 MHz, DMSO-d_6) δ 7.36 (s, 1H), 7.62 (d, J = 8.5 Hz, 2H), 7.77 (d, J = 8.5 Hz, 2H), 8.06 (d, J = 8.7 Hz, 2H), 8.25 (d, J = 8.7 Hz, 2H), 13.80 (br s, NH) ppm. ^{13}C NMR (75 MHz, DMSO-d_6) δ 101.54, 121.21, 124.17, 125.87, 127.20, 131.83, 146.45 ppm. HRMS $(M)^+$ calcd for $C_{15}H_{10}ClN_3O_2$ 299.0462; found 299.0459.

4.1.11. 5-(4-Nitrophenyl)-3-(4-(trifluoromethyl)phenyl)-1*H*-pyrazole (11)

Compound **11** was synthesized from the procedure described for **1**. Mp 244 °C. ^{1}H NMR (300 MHz, DMSO-d_6) δ 7.58 (s, 1H), 7.84 (d, J = 8.3 Hz, 2H), 8.06 (d, J = 8.3 Hz, 2H), 8.12 (d, J = 8.8 Hz, 2H), 8.33 (d, J = 8.8 Hz, 2H), 13.93 (br s, NH) ppm. ^{13}C NMR (75 MHz, DMSO-d_6) δ 102.45, 124.29, 125.72, 125.93, 128.19, 146.61 ppm. HRMS $(M)^+$ calcd for $C_{16}H_{10}F_3N_3O_2$ 333.0725; found 333.0730.

4.1.12. 4-(3-Phenyl-1*H*-pyrazol-5-yl)aniline (12)

To a solution of **1** (0.265 g, 1.0 mmol) in methanol (5 ml), palladium on charcoal (5 mg, 10% w/w) was added. The mixture was treated with hydrogen under atmospheric pressure for 16 h and filtered. The filtrate was evaporated in vacuo and purified with silica gel chromatography (ethyl acetate/hexane = 1:4) to yield **12**. Mp 163 °C. ^{1}H NMR (300 MHz, DMSO-d_6) δ 5.58 (br s, NH_2), 6.64 (d, J = 8.4 Hz, 2H), 6.90 (s, 1H), 7.29 (t, J = 7.3 Hz, 1H), 7.34 (dd, J = 7.7, 7.3 Hz, 2H), 7.52 (d, J = 8.4 Hz, 2H), 7.81 (d, J = 7.7 Hz, 2H), 12.83 (br s, NH) ppm. ^{13}C NMR (75 MHz, DMSO-d_6) δ 97.70, 111.67, 114.21, 125.02, 126.15, 127.42, 127.78, 128.67, 128.82, 148.08 ppm. HRMS $(M)^+$ calcd for $C_{15}H_{13}N_3$ 235.1109; found 235.1113.

4.1.13. 4-(3-(2-Methoxyphenyl)-1*H*-pyrazol-5-yl)aniline (13)

Compound **13** was synthesized from the procedure described for **12**. Mp 158 °C. ^{1}H NMR (300 MHz, DMSO-d_6) δ 3.89 (s, 3H), 7.00 (d, J = 8.3 Hz, 2H), 7.01 (dd, J = 7.8, 7.3 Hz, 1H), 7.02 (s, 1H), 7.11 (d, J = 8.3 Hz, 1H), 7.31 (dd, J = 8.3, 7.8 Hz, 1H), 7.70 (d, J = 8.3 Hz, 2H), 7.79 (d, J = 7.3 Hz, 1H) ppm. ^{13}C NMR (75 MHz, DMSO-d_6) δ 55.48, 101.41, 111.89, 114.15, 118.30, 120.62, 126.15, 127.66, 129.13, 155.87 ppm. HRMS $(M)^+$ calcd for $C_{16}H_{15}N_3O$ 265.1215; found 265.1218.

4.1.14. 4-(3-(3-Methoxyphenyl)-1*H*-pyrazol-5-yl)aniline (14)

Compound **14** was synthesized from the procedure described for **12**. Mp 86 °C. ^{1}H NMR (300 MHz, $CDCl_3$) δ 3.64 (s, 3H), 5.80 (br s, NH_2), 6.57 (d, J = 8.3 Hz, 2H), 6.63 (s, 1H), 6.81 (d, J = 7.7 Hz, 1H), 7.26 (dd, J = 7.7, 4.8 Hz, 1H), 7.27 (s, 1H), 7.27 (d, J = 4.8 Hz, 1H), 7.42 (d, J = 8.3 Hz, 2H), 12.82 (br s, NH) ppm. ^{13}C NMR (75 MHz, $CDCl_3$) δ 55.27, 99.11, 110.67, 114.24, 115.43, 118.36, 121.41, 126.96, 129.85, 133.55, 146.68, 147.94, 149.72, 160.01 ppm. HRMS $(M)^+$ calcd for $C_{16}H_{15}N_3O$ 265.1215; found 265.1217.

4.1.15. 4-(3-(4-Methoxyphenyl)-1*H*-pyrazol-5-yl)aniline (15)

Compound **15** was synthesized from the procedure described for **12**. Mp 173 °C. ^{1}H NMR (300 MHz, DMSO-d_6) δ 3.77 (s, 3H), 5.25 (br s, NH_2), 6.61 (d, J = 8.5 Hz, 2 H), 6.78 (s, 1H), 6.97 (d, J = 8.7 Hz, 2H), 7.46 (d, J = 8.5 Hz, 2H), 7.72 (d, J = 8.7 Hz, 2H), 12.84 (br s, NH) ppm. ^{13}C NMR (75 MHz, DMSO-d_6) δ 55.14, 97.02, 113.88, 114.09, 126.12, 126.35, 148.61, 158.75 ppm. HRMS $(M)^+$ calcd for $C_{16}H_{15}N_3O$ 265.1215; found 265.1218.

4.1.16. 4-(3-(3,4-Dimethoxyphenyl)-1*H*-pyrazol-5-yl)aniline (16)

Compound **16** was synthesized from the procedure described for **12**. Mp 105 °C. ^{1}H NMR (300 MHz, DMSO-d_6) δ 3.77 (s, 3H), 3.80 (s, 3H), 5.27 (br s, NH_2), 6.60 (d, J = 8.3 Hz, 2H), 6.84 (s, 1H), 6.98 (d, J = 8.4 Hz, 1H), 7.32 (d, J = 8.4 Hz, 1H), 7.38 (s, 1H), 7.46 (d, J = 8.3 Hz, 2H), 12.82 (br s, NH) ppm. ^{13}C NMR (75 MHz, DMSO-d_6) δ 55.54, 97.30, 108.93, 112.01, 113.88, 117.52, 126.13, 148.41, 148.58, 148.90 ppm. HRMS $(M)^+$ calcd for $C_{17}H_{17}N_3O_2$ 295.1321; found 295.1325.

4.1.17. 4-(3-(4-(Trifluoromethyl)phenyl)-1*H*-pyrazol-5-yl)aniline (17)

Compound **17** was synthesized from the procedure described for **12**. Mp 266 °C. ^{1}H NMR (300 MHz, DMSO-d_6) δ 5.33 (br s, NH_2), 6.61 (d, J = 8.4 Hz, 2H), 7.02 (s, 1 H), 7.46 (d, J = 8.4 Hz, 2H), 7.76 (d, J = 8.2 Hz, 2H), 8.02 (d, J = 8.2 Hz, 2H), 13.18 (br s, NH) ppm. ^{13}C NMR (75 MHz, DMSO-d_6) δ 98.27, 113.92, 122.61, 125.48, 126.27, 127.52, 148.98 ppm. HRMS $(M)^+$ calcd for $C_{16}H_{12}F_3N_3$ 303.0983; found 303.0984.

4.1.18. *N*,*N*-Dimethyl-4-(3-(4-(trifluoromethyl)phenyl)-1*H*-pyrazol-5-yl)aniline (18)

Compound **18** was synthesized from the procedure described for **1**. Mp 248 °C. ^{1}H NMR (300 MHz, DMSO-d_6) δ 2.92 (s, 6H), 6.77 (d, J = 8.2 Hz, 2H), 7.07 (s, 1H), 7.63 (d, J = 8.2 Hz, 2H), 7.75 (d, J = 7.8 Hz, 2H), 8.04 (d, J = 7.8 Hz, 2H), 13.26 (br s, NH) ppm. ^{13}C NMR (75 MHz, DMSO-d_6) δ 39.97, 98.52, 112.32, 116.94, 122.67, 125.60, 126.19, 127.62, 129.87, 137.94, 144.65, 149.76, 150.25 ppm.HRMS $(M)^+$ calcd for $C_{18}H_{16}F_3N_3$ 331.1296; found 331.1299.

4.1.19. 5-(4-Methoxyphenyl)-3-phenyl-1*H*-pyrazole (19)

Compound **19** was synthesized from the procedure described for **1**. Mp 178 °C. ^{1}H NMR (300 MHz, DMSO-d_6) δ 3.77 (s, 3H), 7.00 (d, J = 8.0 Hz, 2H), 7.06 (s, 1H), 7.32 (t, J = 7.0, 1H), 7.43 (dd, J = 7.2, 7.0, 2H), 7.77 (d, J = 8.0 Hz, 2H), 7.84 (d, J = 7.2, 2H), 13.30 (br s, NH) ppm. ^{13}C NMR (75 MHz, DMSO-d_6) δ 55.13, 98.80, 114.21, 125.08, 126.48, 127.62, 128.73, 158.99 ppm. HRMS $(M)^+$ calcd for $C_{16}H_{14}N_2O$ 250.1106; found 250.1101.

4.1.20. 3-(4-Methoxyphenyl)-5-(4-(trifluoromethyl)phenyl)-1*H*-pyrazole (20)

Compound **20** was synthesized from the procedure described for **1**. Mp 221 °C. ^{1}H NMR (300 MHz, DMSO-d_6) δ 3.78 (s, 3H), 7.03 (d, J = 8.6 Hz, 2H), 7.20 (s, 1H), 7.75 (d, J = 8.6 Hz, 2H), 7.77 (d, J = 8.0 Hz, 2H), 8.04 (d, J = 8.0 Hz, 2H), 13.43 (br s, NH) ppm. ^{13}C NMR (75 MHz, DMSO-d_6) δ 55.18, 99.43, 114.03, 114.41, 121.70, 125.51, 125.88, 126.55, 127.51, 137.66, 143.69, 149.74, 159.27 ppm. HRMS $(M)^+$ calcd for $C_{17}H_{13}F_3N_2O$ 318.0980; found 318.0987.

4.1.21. 4-(3-(4-(Trifluoromethyl)phenyl)-1*H*-pyrazol-5-yl)phenol (21)

A solution of **20** (0.32 g, 1.0 mmol) in CH_2Cl_2 (10 ml) was cooled to −70 °C under argon, and boron tribromide (1.0 g, 2.0 mmol) was added. The mixture was allowed to warm up to room temperature over a period of 16 h and was then cooled to −70 °C. Methanol (10 ml) was added to the reaction mixture, and the solution was evaporated in vacuo and purified with silica gel chromatography (ethyl acetate/hexane = 1:4) to afford **21**. Mp 207 °C. ^{1}H NMR (300 MHz, DMSO-d_6) δ 6.84 (d, J = 8.5 Hz, 2H), 7.13 (s, 1H), 7.62 (d, J = 8.5 Hz, 2H), 7.78 (d, J = 8.2 Hz, 2H), 8.03 (d, J = 8.2 Hz, 2H), 9.65 (br s, OH), 13.30 (br s, NH) ppm. ^{13}C NMR (75 MHz, DMSO-d_6) δ 99.28, 115.65, 125.51, 125.61, 125.66, 126.65, 126.59, 157.53 ppm. HRMS $(M)^+$ calcd for $C_{16}H_{11}F_3N_2O$ 304.0823; found 304.0825.

4.1.22. 3-(4-Fluorophenyl)-5-(4-methoxyphenyl)-1*H*-pyrazole (22)

Compound **22** was synthesized from the procedure described for **1**. Mp 203 °C. ^{1}H NMR (300 MHz, DMSO-d_6) δ 3.78 (s, 3H), 7.01 (d, J = 8.4 Hz, 2H), 7.04 (s, 1H), 7.26 (dd, J = 7.6, 2.1 Hz, 2H), 7.74 (d, J = 8.4 Hz, 2H), 7.85 (dd, J = 7.6, 2.1 Hz, 2H), 13.22 (br s, NH) ppm. ^{13}C NMR (75 MHz, DMSO-d_6) δ 55.14, 98.71, 114.31, 121.98, 126.48, 126.99, 127.09, 159.10 ppm. HRMS $(M)^+$ calcd for $C_{16}H_{13}FN_2O$ 268.1012; found 268.1016.

4.1.23. 3-(4-Chlorophenyl)-5-(4-methoxyphenyl)-1*H*-pyrazole (23)

Compound **23** was synthesized from the procedure described for **1**. Mp 221 °C. ^{1}H NMR (300 MHz, DMSO-d_6) δ 3.78 (s, 3H), 7.01 (d, J = 7.9 Hz, 2H), 7.09 (s, 1H), 7.49 (d, J = 7.2 Hz, 2H), 7.73 (d, J = 7.9 Hz, 2H), 7.84 (d, J = 7.2 Hz, 2H), 13.26 (br s, NH) ppm. ^{13}C NMR (75 MHz, DMSO-d_6) δ 55.33, 99.11, 114.47, 121.96, 126.68, 126.92, 128.86, 159.27 ppm. HRMS $(M)^+$ calcd for $C_{16}H_{13}FN_2O$ 284.0716; found 284.0713.

4.1.24. 3-(4-Bromophenyl)-5-(4-methoxyphenyl)-1*H*-pyrazole (24)

Compound **24** was synthesized from the procedure described for **1**. Mp 223 °C. ^{1}H NMR (300 MHz, DMSO-d_6) δ 3.78 (s, 3H), 7.01 (d, J = 8.7 Hz, 2H), 7.08 (s, 1H), 7.61 (d, J = 8.4 Hz, 2H), 7.74 (d, J = 8.7 Hz, 2H), 7.78 (d, J = 8.4 Hz, 2H), 13.29 (br s, NH) ppm. ^{13}C NMR (75 MHz, DMSO-d_6) δ 55.17, 99.02, 114.29, 120.54, 126.49, 127.04, 131.64, 159.10 ppm. HRMS $(M)^+$ calcd for $C_{16}H_{13}BrN_2O$ 328.0211; found 328.0208.

4.1.25. 3-(4-Methoxyphenyl)-5-(naphthalen-2-yl)-1*H*-pyrazole (25)

Compound **25** was synthesized from the procedure described for **1**. Mp 266 °C. ^{1}H NMR (300 MHz, DMSO-d_6) δ 3.80 (s, 3H), 7.03 (d, J = 8.4 Hz, 2H), 7.22 (s, 1H), 7.51 (d, J = 5.9 Hz, 1H), 7.55 (d, J = 5.9 Hz, 1H), 7.78 (d, J = 8.4 Hz, 2H), 7.92 (d, J = 7.3 Hz, 2H), 7.97 (d, J = 7.3 Hz, 2H), 8.35 (s, 1H), 13.30 (br s, NH) ppm. ^{13}C NMR (75 MHz, DMSO-d_6) δ 55.17, 99.04, 114.41, 123.33, 125.73, 126.49, 127.63, 127.91, 132.45, 133.20, 143.47, 151.12, 159.17 ppm. HRMS $(M)^+$ calcd for $C_{20}H_{16}N_2O$ 300.1263; found 300.1264.

4.1.26. 3-(Biphenyl-2-yl)-5-(4-methoxyphenyl)-1*H*-pyrazole (26)

Compound **26** was synthesized from the procedure described for **1**. Mp 159 °C. ^{1}H NMR (300 MHz, DMSO-d_6) δ 3.74 (s, 3H), 5.89 (s, 1H), 6.92 (d, J = 8.4 Hz, 2H), 7.21–7.24 (m, 2H), 7.30–7.35 (m, 4H), 7.45(d, J = 8.4 Hz, 2H), 7.45(m, 2H), 7.68 (s, 1H), 12.80, 13.07 (br s, NH) ppm. ^{13}C NMR (75 MHz, DMSO-d_6) δ 55.09, 101.39, 114.18, 126.18, 126.94, 127.46, 128.01, 129.08, 129.17, 130.38, 140.30, 158.84 ppm. HRMS $(M)^+$ calcd for $C_{22}H_{18}N_2O$ 326.1419; found 326.1425.

4.1.27. 3-(Biphenyl-2-yl)-5-(4-(trifluoromethyl)phenyl)-1*H*-pyrazole (27)

Compound **27** was synthesized from the procedure described for **1**. Mp 170 °C. ^{1}H NMR (300 MHz, DMSO-d_6) δ 6.19 (s, 1H), 7.20–7.24 (m, 2H), 7.31–7.36 (m, 3H), 7.37(m, 1H), 7.40 (m, 2H), 7.64 (s, 1H), 7.72 (d, J = 7.8 Hz, 2H), 7.79 (d, J = 7.8 Hz, 2H), 13.29 (br s, NH) ppm. ^{13}C NMR (75 MHz, DMSO-d_6) δ 103.22, 125.35, 125.58, 125.99, 126.85, 127.18, 127.43, 127.64, 128.84, 129.00, 129.43, 130.51, 137.51, 140.50, 140.57, 143.14, 148.74 ppm. HRMS $(M)^+$ calcd for $C_{20}H_{16}N_2O$ 364.1187; found 364.1197.

4.1.28. 3-(Biphenyl-2-yl)-5-(2-methoxyphenyl)-1*H*-pyrazole (28)

Compound **28** was synthesized from the procedure described for **1**. Mp 122 °C. ^{1}H NMR (300 MHz, DMSO-d_6) δ 3.72 (s, 3H), 6.00 (s, 1H), 6.94 (dd, J = 7.4, 7.3 Hz, 1H), 7.03 (d, J = 8.2 Hz, 1H), 7.22 (dd, J = 8.2, 7.3 Hz, 1H), 7.22–7.25 (m, 2H), 7.34 (m, 4H), 7.42 (d, J = 7.4 Hz, 1H), 7.42 (m, 2H), 7.78 (s, 1H), 12.93 (br s, NH) ppm. ^{13}C NMR (75 MHz, DMSO-d_6) δ 55.14, 105.13, 111.88, 117.78, 120.57, 126.80, 127.04, 127.41, 128.03, 128.50, 129.12, 130.37, 132.63, 138.60, 140.17, 141.82, 150.21, 155.41 ppm. HRMS $(M)^+$ calcd for $C_{22}H_{18}N_2O$ 326.1419; found 326.1424.

4.1.29. 3-(Biphenyl-2-yl)-5-(3-methoxyphenyl)-1*H*-pyrazole (29)

Compound **29** was synthesized from the procedure described for **1**. Mp 63 °C. ^{1}H NMR (300 MHz, DMSO-d_6) δ 3.75 (s, 3H), 6.00 (s, 1H), 6.84 (d, J = 7.2 Hz, 1H), 7.15 (s, 1H), 7.15 (d, J = 6.8 Hz, 1H), 7.21–7.27 (m, 2H), 7.24 (dd, J = 7.2, 6.8 Hz, 1H), 7.30–7.37 (m, 4H), 7.46 (m, 2H), 7.69 (s, 1H), 12.93, 13.25 (br s, NH) ppm. ^{13}C NMR (75 MHz, DMSO-d_6) δ 55.04, 102.77, 110.32, 113.07, 117.30, 126.98, 127.50, 128.05, 129.09, 129.22, 129.88, 130.39, 140.37, 159.55 ppm. HRMS $(M)^+$ calcd for $C_{22}H_{18}N_2O$ 326.1419; found 326.1421.

4.1.30. 2-(3-(Biphenyl-2-yl)-1*H*-pyrazol-5-yl)phenol (30)

Compound **30** was synthesized from the procedure described for **21**. Mp 135 °C. ^{1}H NMR (300 MHz, DMSO-d_6) δ 6.28 (s, 1H), 6.81 (dd, J = 7.4, 7.3 Hz, 1H), 6.89 (d, J = 8.0 Hz, 1H), 7.12 (dd, J = 8.0, 7.4 Hz, 1H), 7.22–7.24 (m, 2H), 7.31–7.33 (m, 3H), 7.42–7.48 (m, 3H), 7.46 (d, J = 7.3 Hz, 1H), 7.66 (s, 1H), 10.83 (br s, OH), 13.21 (br s, NH) ppm. ^{13}C NMR (75 MHz, DMSO-d_6) δ 102.96, 116.42, 116.98, 119.27, 126.59, 127.20, 127.66, 128.18, 128.82, 129.07, 129.65, 130.56, 140.71, 142.68, 150.29, 155.21 ppm. HRMS $(M)^+$ calcd for $C_{21}H_{16}N_2O$ 312.1263; found 312.1260.

4.1.31. 4-(3-(Biphenyl-2-yl)-1*H*-pyrazol-5-yl)phenol (31)

Compound **31** was synthesized from the procedure described for **21**. Mp 119 °C. ^{1}H NMR (300 MHz, DMSO-d_6) δ 5.84 (s, 1H), 6.74 (d, J = 8.3 Hz, 2H), 7.21–7.23 (m, 2H), 7.27–7.36 (m, 3H), 7.34 (d, J = 8.3 Hz, 2H), 7.41–7.45 (m, 3H), 7.69 (s, 1H), 9.59 (br s, OH), 12.75, 13.00 (br s, NH) ppm. ^{13}C NMR (75 MHz, DMSO-d_6) δ 101.50, 115.52, 126.27, 126.93, 127.45, 128.01, 129.09, 129.18, 130.38, 140.27, 157.14 ppm. HRMS $(M)^+$ calcd for $C_{21}H_{16}N_2O$ 312.1263; found 312.1264.

4.1.32. 3-(Biphenyl-2-yl)-5-(4-nitrophenyl)-1*H*-pyrazole (32)

Compound **32** was synthesized from the procedure described for **1**. Mp 213 °C. ^{1}H NMR (300 MHz, DMSO-d_6) δ 6.31 (s, 1H), 7.20–7.24 (m, 2H), 7.31–7.36 (m, 3H), 7.44(m, 1H), 7.50–7.52 (m, 2H), 7.60 (s, 1H), 7.87 (d, J = 8.7 Hz, 2H), 8.22 (d, J = 8.7 Hz, 2H), 13.29 (br s, NH) ppm. ^{13}C NMR (75 MHz, DMSO-d_6) δ 103.84, 124.11, 125.59, 125.98, 127.20, 127.64, 128.14, 128.99, 129.54, 130.51, 140.00, 140.38, 140.60, 143.45, 146.28, 148.24 ppm. HRMS $(M)^+$ calcd for $C_{21}H_{15}N_3O_2$ 341.1164; found 341.1165.

4.1.33. 4-(3-(Biphenyl-2-yl)-1*H*-pyrazol-5-yl)aniline (33)

Compound **33** was synthesized from the procedure described for **12**. Mp 93 °C. ^{1}H NMR (300 MHz, DMSO-d_6) δ 5.22 (br s, NH_2), 5.74(s, 1H), 6.52 (d, J = 8.4 Hz, 2H), 7.19–7.24 (m, 2H), 7.24 (d, J = 8.4 Hz, 2H), 7.27–7.33 (m, 4H), 7.38–7.43 (m, 2H), 7.70 (s, 1H), 12.81 (br s, NH) ppm. ^{13}C NMR (75 MHz, DMSO-d_6) δ 100.70, 113.81, 125.86, 126.84, 127.37, 127.66, 127.96, 129.09, 130.34, 140.19, 141.55, 148.52 ppm. HRMS $(M)^+$ calcd for C21H17N3 311.1422; found 311.1418.

4.2. Cell culture

Cancer cells were purchased from Bioresource Collection and Research Center in, Hsinchu, Taiwan. Each cell line was maintained in the standard medium and grown as a monolayer in Dulbecco's Modified Eagle Medium (DMEM) containing 10% fetal bovine serum, 2 mM glutamine, 100 units/ml penicillin, and 100 g/ml streptomycin. Cultures were maintained at 37 °C with 5% CO_2 in a humidified atmosphere.

4.3. MTT assay for cell viability

OVCA, SW620, H460 and AGS cells were plated in 96-well microtiter plates at a density of 3000, 3000, 3000 and 5000 cells/well, respectively. After 24 h incubation, cells were treated with vehicle alone (control) or compounds (drugs were dissolved in DMSO previously) at the concentrations indicated. Treated cells were further incubated for 48 h. Cell survival is expressed as percentage of control cell growth. The 3-[4,5-dimethylthiazol-2-yl]-2,5-diphenyltetrazolium bromide (MTT, 2 mg/ml) dye reduction assay in 96-well microplates was used. The assay is dependent on the reduction of MTT by mitochondrial dehydrogenases of viable cell to a blue formazan product, which come be measured spectrophotometrically. Tumor cells were incubated in each well

with serial dilutions of the tested compounds. After two days of incubation (37 °C, 5% CO_2 in a humid atmosphere) 100 μl of MTT (2 mg/ml in PBS) was added to each well and the plate was incubated for a further 2 h (37 °C). The resulting formazan was dissolved in 100 μl DMSO and read at 570 nm. The percentage of growth inhibition was calculated by the following equation: percentage growth inhibition = $(1 \times At/Ac) \times 100$, where At and Ac represent the absorbance in treated and control cultures, respectively. The drug concentration causing a 50% cell growth inhibition (GI_{50}) was determined by interpolation from dose–response curves. All determinations were carried out in four to six separated experiments.

4.4. Determination of apoptosis by flow cytometry

Apoptosis and cell cycle profile were assessed by DNA fluorescence flow cytometry. OVCA cells treated with 0.5% DMSO or tested compounds at indicated concentrations for 24 h were harvested, rinsed in PBS, resuspended and fixed in 80% ethanol, and stored at −20 °C in fixation buffer until ready for analysis. Then the pellets were suspended in 1 ml of fluorochromic solution (0.08 mg/ml PI (propidium iodide), 0.1% TritonX-100 and 0.2 mg/ml RNase A in 1× PBS) at room temperature in the dark for 30 min. The DNA content was analyzed by FACScan flow cytometer (Becton Dickinson, Mountain View, CA) and CELLQUEST software (Becton Dickinson). The population of apoptotic nuclei (subdiploid DNA peak in the DNA fluorescence histogram) was expressed as the percentage in the entire population.

4.5. Protein extraction and Western blotting

After the treatment of cells with vehicle (1% DMSO), **26** and **27** for indicated time treatment, the cells were washed twice with PBS and reaction was terminated by the addition of 100 μl lysis buffer. For Western blot analysis, the amount of proteins (50 μg) were separated by electrophoresis in a 15% SDS–PAGE and transferred to a nitrocellulose membrane. After an overnight incubation at 4 °C in TBST/5% non-fat milk, the membrane was washed with TBST three times and immuno-reacted with the monoclonal primary antibodies, anti-beta-actin (1:1000), anti-poly-ADP-ribose polymerase(PARP) (1:500), anti-cleaved caspase-3 (1:1000), anti-cleaved caspase-9 (1:1000), anti-phospho-Akt (1:1000), anti-Akt (1:1000) from Cell Signaling Technology (Beverly, MA) were used. After four washings with TBST, the anti-mouse or anti-rabbit IgG (dilute 1:10,000) was applied to the membranes for 1 h at room temperature. The membranes were washed with TBST for 1 h and the detection of signal was performed with an enhanced chemiluminescence (ECL) detection reagents.

4.6. Statistical analysis

Data are presented as means ± SEM (standard error of the mean) from three independent experiments. Statistical analyses used the Bonferroni *t*-test after ANOVA for multi-group comparison and Student's *t*-test for two-group comparison. $P < 0.05$ was considered significant.

4.7. CoMFA 3D-QSAR analysis

CoMFA (Comparative Molecular Field Analysis) was carried out by software Sybyl 8.1 (Tripos International, St. Louis, Missouri, USA). MMFF94 charge assignment and force field were applied to prepare compound structures. The geometries were minimized by Powell algorithm to an energy convergence criterion of 0.01 kcal/mol Å, within 100,000 iterations. Each compound in its energetically minimized geometry was aligned. Two CoMFA descriptors including steric (Lennard–Jones 6–12 potential) and electrostatic (Coulombic potential) field energies were calculated with a sp^3 carbon atom carrying +1.0 charge to serve as a probe atom using Sybyl default parameters. The optimal number of components (ONC = 2) was recommended after a leave-one-out cross-validated run. The final training set model and coefficients such as non-validation R^2 and *F*-value were obtained by using the optimal number of components and all the data points in the training set. The cross-validated $q^2 = 0.671$ and the subsequent non-validation $R^2 = 0.846$ meet the criteria $q^2 \geqq 0.5$ and $R^2 \geqq 0.8$. The contributions for steric and electrostatic fields are 0.459 and 0.561, respectively.

Acknowledgments

Financial support from the National Science Council of the Republic of China and Tamkang University to A. Y. Shaw is gratefully acknowledged.

References and notes

1. Wyllie, A. H.; Kerr, J. F.; Currie, A. R. *Int. Rev. Cytol.* **1980**, *68*, 251.
2. Thompson, C. *Science* **1995**, *267*, 1456.
3. Alnemri, E. S.; Livingston, D. J.; Nicholson, D. W.; Salvesen, G.; Thornberry, N. A.; Wong, W. W.; Yuan, J. *Cell* **1996**, *87*, 171.
4. Thornberry, N.; Lazebnik, Y. *Science* **1998**, *281*, 1312.
5. Parameswaran, P. S.; Naik, C. G.; Hegde, V. R. *J. Nat. Prod.* **1997**, *60*, 802.
6. Biere, H.; Boettcher, I.; Kapp, J. F. *Arch. Pharm.* **1983**, *316*, 588.
7. Penning, T. D.; Talley, J. J.; Bertenshaw, S. R.; Carter, J. S.; Collins, P. W.; Docter, S.; Graneto, M. J.; Lee, L. F.; Malecha, J. W.; Miyashiro, J. M.; Rogers, R. S.; Rogier, D. J.; Yu, S. S.; Anderson, G. D.; Burton, E. G.; Cogburn, J. N.; Gregory, S. A.; Koboldt, C. M.; Perkins, W. E.; Seibert, K.; Veenhuizen, A. W.; Zhang, Y. Y.; Isakson, P. C. *J. Med. Chem.* **1997**, *40*, 1347.
8. Zhang, J.; Shen, B.; Lin, A. *Trends Pharmacol. Sci.* **2007**, *28*, 286.
9. Zhou, H.-B.; Carlson, K. E.; Stossi, F.; Katzenellenbogen, B. S.; Katzenellenbogen, J. A. *Bioorg. Med. Chem. Lett.* **2009**, *19*, 108.
10. Chimenti, F.; Fioravanti, R.; Bolasco, A.; Manna, F.; Chimenti, P.; Secci, D.; Befani, O.; Turini, P.; Ortuso, F.; Alcaro, S. *J. Med. Chem.* **2007**, *50*, 425.
11. Knorr, L.; Duden, P. B. *Dtsch. Chem. Ges.* **1893**, *26*, 111.
12. Beam, C. F.; Foote, R. S.; Hauser, C. R. *J. Chem. Soc. Sect. C: Org.* **1971**, *9*, 1658.
13. Heller, S. T.; Natarajan, S. R. *Org. Lett.* **2006**, *8*, 2675.
14. Mosman, T. J. *Immunol. Methods* **1983**, *65*, 55.
15. Vivanco, I.; Sawyers, C. L. *Nat. Rev. Cancer* **2002**, *2*, 489.